Blue moon ensemble simulation of aquation free energy profiles applied to mono and bifunctional platinum anticancer drugs

Teruo Hirakawa,[1,2] David R. Bowler,[3,4,5] Tsuyoshi Miyazaki,[6,5] Yoshitada Morikawa,[1,7,8] and Lionel A. Truflandier[2,1,a]

[1] *Department of Precision Science and Technology, Graduate School of Engineering, Osaka University, 2-1, Yamada-oka, Suita, Osaka 565-0871, Japan*

[2] *Institut des Sciences Moléculaires (ISM), Université Bordeaux, CNRS UMR 5255, 351 cours de la Libération, 33405 Talence cedex, France*

[3] *Department of Physics & Astronomy, University College London (UCL), Gower St, London, WC1E 6BT, UK*

[4] *London Centre for Nanotechnology, UCL, 17-19 Gordon St, London WC1H 0AH, UK*

[5] *Centre for Materials Nanoarchitechtonics (MANA), National Institute for Materials Science (NIMS), 1-1 Namiki, Tsukuba, Ibaraki 305-0044, Japan*

[6] *Computational Materials Science Unit (CMSU), NIMS, 1-1 Namiki, Tsukuba, Ibaraki 305-0044, Japan*

[7] *Elements Strategy Initiative for Catalysts and Batteries (ESICB), Kyoto University, Katsura, Kyoto 615-8520, Japan*

[8] *Research Center for Ultra-Precision Science and Technology, Graduate School of Engineering, Osaka University, 2-1, Yamada-oka, Suita, Osaka 565-0871, Japan*

(Dated: 4 March 2020)

Aquation free energy profiles of neutral cisplatin and cationic monofunctional derivatives, including triaminochloroplatinum(II) and cis-diammine(pyridine)chloroplatinum(II), were computed using state of the art thermodynamic integration, for which temperature and solvent were accounted for explicitly using density functional theory based canonical molecular dynamics (DFT-MD). For all the systems the "inverse-hydration" where the metal center acts as an acceptor of hydrogen bond has been observed. This has motivated to consider the inversely bonded solvent molecule in the definition of the reaction coordinate required to initiate the constrained DFT-MD trajectories. We found that there exists little difference in free enthalpies of activations, such that these platinum-based anticancer drugs are likely to behave the same way in aqueous media. Detailed analysis of the microsolvation structure of the square-planar complexes, along with the key steps of the aquation mechanism are discussed.

I. INTRODUCTION

The discovery of the anticancer activity of cisplatin (Scheme 1) during the 60's has promoted fast development of platinum(II)-based drugs which are currently found in chemotherapy regimens (see Refs. 1–4 for reviews). Despite few successes for some of them in curing specific cancers, eg. the treatment of testicular cancer with cisplatin, their efficiency against the broad spectrum of carcinoma remains limited. The main challenges to overcome are: (1) the elimination of the severe side effects related to their poor selectivity

---

[a] Electronic mail: lionel.truflandier@u-bordeaux.fr

with respect to the tumor cells, and (2) the resistance —either intrinsic (static) or evolution-ary (dynamic)—, observed for some types of cancer.[5–7] Solving the first problem requires the design of new drug delivery strategies,[3,4] which ideally prevents the degradation of platinum complex in the blood stream and allows for a precise targeting of the tumor tissue. Solution to the second problem implies heuristic methods, such as the structure-activity relationship (SAR),[2,8] from which a huge number[8] of platinum(II)-based drugs and platinum(IV)-based prodrugs were synthesized and tested as many attempts to mimic the cisplatin's mechanism of action while trying to improve the cytotoxic properties. As a result of 30 years of trial and error less than 30 platinum drugs have been considered for clinical trials, with only 2 of them (carboplatin and oxaliplatin) approved wordwilde for clinical used.[1,4] Whereas high-throughput synthesis and screening[9] of drug candidates may provide rapid —but partial— solutions to an urgent problem, understanding and controlling every details of cisplatin's mechanism constitutes a safer —but far more longer— route towards a rational design of a universal platinum-based anticancer molecule. The process by which cisplatin (and bifunc-tional derivatives) leads to cell death is now rather well understood.[10,11] It is divided into 4 main steps: (i) the cellular uptake, (ii) the aquation/activation (Scheme 1) in the cellular media, (iii) the DNA platination, that is, bifunctional intra- and interstrand crossed-links *via* the fomation of 2 covalent bonds between the metal center and the purine bases, and (iv) the DNA-damage recognition initiating apoptosis, or cell-cycle arrest eventually followed by an attempt to repair the lesion. In elucidating each step of the mechanism, atomistic computations and simulations based on either (classical) molecular, quantum, or mixed molecular/quantum mechanics can provide important insights.

FIG. 1. Aquation reaction of cisplatin (**1**) and monofunctional derivatives (**2**).

At the pure quantum mechanics level of theory, some of the efforts were devoted to investigate the hydration structure of the square-planar Pt-complexes[12–14] in response to some experimental evidence[15,16] showing unusual bonding situation —referred as to inverse-hydration— where the Pt atom acts as a hydrogen-bond acceptor. Energetic contributions[17–19] and topological analysis,[20] along with minute details on the influence of the bulk solvation effects have been extensively discussed in literature.[19,21,22] Another interest which is also closely related to our concern is the activation of cisplatin after the cellular uptake of the platinum drug. The aquation reaction (also loosely called hydrolysis) represented on Scheme 1 through the substitution of one or both chloride ligands of cisplatin by water molecules was recognized as a crucial step to initiate DNA platination.[23] The proof of concept is carboplatin[24–26] featuring the cyclobutanedicarboxylate in replacement of the chloride leaving ligands of cisplatin. It demonstrates much more slower aquation and DNA platination rates but displayed similar crossed-link sites.[27]

To access more details on the aquation of cisplatin and derivatives, many theoretical works have focused on computing activation barriers using static molecular clusters and implicit solvation models.[28] When applied for modelling aqueous reactions, insights arising from this type of computations remain limited since they do not account properly for the
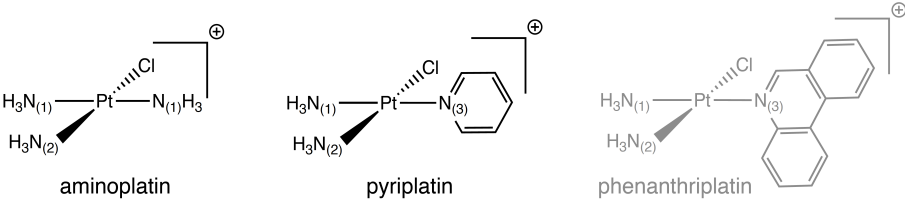
FIG. 2. Structures cationic monofunctional platinum complexes. Note that phenantriplatin has not been investigated in this work.

dynamic reorganisation of solvation shell surrounding the molecule, especially when the solvent is one of the reactant. More advanced but computationally demanding methods can be envisaged where bulk and microsolvation effect are treated on equal footing using density functional theory molecular dynamics (DFT-MD) along with free energy path evaluation based on metadynamics further refined by umbrella sampling.[29,30] Alternatives to DFT-MD, such as the reference interaction site model self-consistent field[31,32] (RISM-SCF) can also be employed.[33]

From the last ten-years research focussing on reducing the tumor-cell resistance to bi-functional cisplatin and derivatives, it has been shown that monofunctional analogues[34–36] can be considered as potent candidates.[37–39] Monofunctional platinum(II)-based drugs are cationic square-planar complexes (Scheme. 2) of formula $[Pt(NH_3)_2(N\text{-heterocycle})Cl]^+$, deriving from the triammine-chloro precursor $[Pt(NH_3)_3Cl]^+$, later referred as to aminoplatin. In a systematic investigation of the cancer-cell responses with respect to the heterocyclic N-donor ligand bound to the metal, it has been demonstrated[40] that the size and the arrangement of the aromatic rings affects drastically the cytotoxic and selectivity properties of the monofunctional platinum(II) drugs. As a matter of fact, whereas aminoplatin was found to be biologically inactive, phenanthriplatin, and to a lesser extent pyriplatin, presents a remarkable potency,[41] exceeding in the majority of the cases the anticancer activity of cisplatin.[40,41]

This work aims to investigate the aquation reaction of Pt(II) complexes using state of the art thermodynamic integration coupled to DFT-MD simulations to determine if cationic monofunctional derivatives present differences in the free energy profiles and mechanism of reaction. The paper is organized as following: Section 2 provides methodological and computational aspects related to the DFT-BOMD simulation and blue moon ensemble (BME) integration. Results and discussion are presented in Section 3. The paper concludes with a brief summary of the key findings and an outlook.

II. COMPUTATIONAL DETAILS

A. DFT-BOMD simulations

All the DFT-MD simulations reported in this article were performed on the Born-Oppenheimer (BO) surface, where the Kohn-Sham (KS) self-consistent-field (SCF) equations are solved at each step of the dynamics using the CONQUEST code.[42–44] A strictly localized (atomic-like and finite range) numerical double-ζ basis set[45–47] including polarisation functions (DZP) for expanding the valence wavefunctions along with norm-conserving pseudopotentials[48] (NCPP) were especially designed for this work. Thereafter, this basis set will be referred as pseudo-atomic orbitals (PAO). Using a benchmark of isolated Pt complexes, reliability of the PAOs were checked against molecular calculations based on gaussian-type orbitals (GTO). Additional computational parameters related to the PAOs and NCPPs generation along with their assessments can be found in the Sec. S1 of the Supporting Information (SI). The KS-SCF equations were solved within the framework

of the generalized gradient approximation (GGA) of the exchange-correlation functional proposed by Perdew, Burke, and Ernzerhof (PBE).[49] This choice of GGA functional was more pragmatic than idealistic. It is well established (see Refs. 50,51 for recent studies) that the PBE functional yields to a "glassy" state of liquid water at ambient temperature preventing a fully quantitative agreement with experiments. Nevertheless, also important for this work, it has been demonstrated that the same functional is able to reproduce the inverse-hydration feature.[52]

Solvation of the platinum complexes has been modeled using cubic simulation boxes with 63 water molecules adapted in size to reach an average density of 1.0 g·cm^{-3}. For cationic complexes, the excess of positive charge was balanced by substituting water molecule with hydroxide anion keeping the overall charge of the supercell neutral. For the DFT-BOMD simulations, ionic cores were propagated using the velocity Verlet algorithm[53] with a time step of 0.5 fs, for which a SCF convergence criteria of 10^{-7} on the residual of the electronic density, and a grid spacing of about 0.20 au were found sufficient to prevent any energy drift during microcanonical simulations. The same set of convergence parameters were used for NVT-ensemble simulations using a Nosé–Hoover chain[54,55] of 5 thermostats with a frequency of 500 cm^{-1}.

B. Blue moon ensemble integration

The hydrolysis free energy profiles of cisplatin and its derivatives were calculated using thermodynamic integration *via* the blue moon ensemble (BME) technique.[56] Given a reaction coordinate, $\xi \equiv \xi(\{\mathbf{r}_i\})$, which in general depends on a subset of the N atomic positions $\{\mathbf{r}_i\}$, the variation of free energy between some initial state, ξ_0, up to the current value of ξ can be expressed as:

$$\Delta F(\xi, T) = \int_{\xi_0}^{\xi} \left(\frac{\partial F(\xi; T)}{\partial \xi} \right)_{\xi'} d\xi', \tag{1}$$

Integration is performed numerically through the sampling of the reaction coordinate using a discret set of $n_{\xi'}$ target values $\{\xi'\}$. The free energy gradient —also referred to as (minus) the mean force— in Eq. (1) is evaluated for each ξ' from a constrained MD trajectory where $\xi - \xi' = 0$ is enforced. Following BME Lagrangian formulation of Sprik and Ciccotti,[57] the mean force writes

$$\left(\frac{\partial F(\xi; T)}{\partial \xi} \right)_{\xi'} = \frac{\langle Z^{-1/2} \left(-\lambda_\xi + k_B T G \right) \rangle_{\xi'}}{\langle Z^{-1/2} \rangle_{\xi'}}, \tag{2}$$

for which k_B and T are the Boltzmann constant and temperature, respectively. The Lagrange multiplier, λ_ξ, associated with constrained coordinate ξ, defines the strength the constraint force updated at each MD step.[58–60] The remaining terms are given by,

$$Z = \sum_{i=1}^{N} \frac{1}{m_i} \left(\frac{\partial \xi}{\partial \mathbf{r}_i} \right)^2, \tag{3}$$

$$G = \frac{1}{Z^2} \sum_{i=1}^{N} \sum_{j=1}^{N} \frac{1}{m_i m_j} \frac{\partial \xi}{\partial \mathbf{r}_i} \cdot \frac{\partial^2 \xi}{\partial \mathbf{r}_i \mathbf{r}_j} \cdot \frac{\partial \xi}{\partial \mathbf{r}_j}. \tag{4}$$

where m_i designates the mass of the ith nucleus. In Eq. (1), the notation $\langle \cdot \rangle_{\xi'}$ stands for the canonical ensemble average performed for each target value ξ'. Around 20 values were used for the reaction path discretization. Ensemble averages performed at $T = 310$ K were obtained from production runs of 2.5 ps subsequent to 1.0 ps of equilibration. Free energy errors were estimated by the method of Jacucci and Rahman.[61]

III. RESULTS AND DISCUSSION

A. MD analysis and reliability

TABLE I. Comparison of selected structural parameters of the solvated bi and monofunctional cisplatin derivatives obtained with the PBE functional using various methods. For BOMD simulations, mean distance and angle values are given along with their respective standard deviations. Inequivalent nitrogen atoms are numbered according to Schemes 1 and 2.

Complex	Method	Basis	Distance (Å)		Angle (deg)	
cisplatin			Pt–N	Pt–Cl	N–Pt–N	Cl–Pt–Cl
	BOMD-NVE	PAO-DZP	2.08 ± 0.04	2.37 ± 0.03	91.0 ± 4.0	92.5 ± 3.4
	CPMD-NVE^a	PW	2.09 ± 0.04	2.35 ± 0.03	90.4 ± 4.1	92.3 ± 4.3
	Static-PCM^b	GTO-DZP	2.07	2.34	92.7	94.7
	Static	GTO-DZP	2.09	2.30	99.1	95.7
	Static	PAO-DZP	2.10	2.34	98.5	96.0
mono-aqua cisplatin			Pt–N$_{(1)}$[Pt–N$_{(2)}$]	Pt–Cl	Pt–O	N–Pt–N
	BOMD-NVE	PAO-DZP	$2.05[2.08] \pm 0.03[0.05]$	2.36 ± 0.03	2.10 ± 0.07	91.4 ± 4.5
	Static-PCM	GTO-DZP	2.02[2.07]	2.32	2.10	93.5
	Static	GTO-DZP	2.03[2.11]	2.28	2.10	97.2
	Static	PAO-DZP	2.04[2.12]	2.32	2.11	96.6
aminoplatin			Pt–N$_{(1)}$[Pt–N$_{(2)}$]	Pt–Cl	N$_{(1)}$–Pt–N$_{(2)}$	N$_{(1)}$–Pt–Cl
	BOMD-NVE	PAO-DZP	$2.06[2.08] \pm 0.04[0.04]$	2.40 ± 0.03	90.5 ± 4.2	89.5 ± 4.2
	Static-PCM	GTO-DZP	2.06[2.08]	2.33	91.2	88.8
	Static	GTO-DZP	2.07[2.12]	2.28	93.6	86.4
	Static	PAO-DZP	2.08[2.13]	2.32	93.4	86.3
pyriplatin			Pt–N$_{(1)}$[Pt–N$_{(2)}$]	Pt–Cl	Pt–N$_{(3)}$	N$_{(1)}$–Pt–N$_{(2)}$
	BOMD-NVE	PAO-DZP	$2.04[2.07] \pm 0.03[0.04]$	2.37 ± 0.03	2.07 ± 0.03	90.3 ± 4.1
	Static-PCM	GTO-DZP	2.07[2.08]	2.33	2.02	91.3
	Static	GTO-DZP	2.08[2.10]	2.28	2.02	95.0
	Static	PAO-DZP	2.09[2.13]	2.32	2.02	95.0

^{a}Results obtained in Ref. 13 using the Car-Parrinello (CP) approach as implemented in QUANTUM ESPRESSO[62]. The implementation is based on planewave (PW) basis set and pseudopotentials. The same model has been used for the BOMD and CPMD simulations, eg. box size and number of atoms. ^{b}'Static' refers to gas-phase optimized structures including (or not) an implicit water-solvent treatment based on the Polarizable Continuum Model (PCM) as implemented in GAUSSIAN09[63].

To assess the quality of our DFT-BOMD simulations, the liquid structure of the solvated Pt-complexes were analysed *via* the radial distribution function (RDF) —leading to the pair correlation function $g(r)$— and the power spectral density (PSD) of the velocity autocorrelation function (VACF) —leading to the vibrational density of states (VDOS). The methodology used for the calculations of these properties can be found in the SI of Ref. 52. For each system, RDFs (VDOS) were computed from a NVT (NVE) production run of 10 ps performed after a NVT equilibration step of 15 ps. The PSD was refined using the Welch window function with 8 non-overlapping segments of 512 data points.[64] Analysis and a brief discussion of the solvent RDFs and VDOS in light of previous studies are given in Sec. S2 of the SI. Below we shall concentrate on the solute structural and vibrational signatures.

Selected mean bond distances and angles obtained from the microcanonical BOMD simulations are collected in Table I for all the Pt-based reactants investigated in this work. For cisplatin, when compared to previous DFT-MD simulations using the same XC functional but a different implementation,[13] a nice agreement is observed. By comparing across the set of platinum complexes the deviations of the Pt-ligand mean bond distances and angles with respect to gas phase optimized strutures, we can isolate two systematic effects of aqueous solvent: (i) an increase of the Pt−Cl bond length, (ii) a net decrease of the N−Pt−N angles. Analyses of the $g(r)$ associated to the solvent-solute interactions given in Figure 3 allows for interpreting the systematic effects in terms of ligand hydration shells.

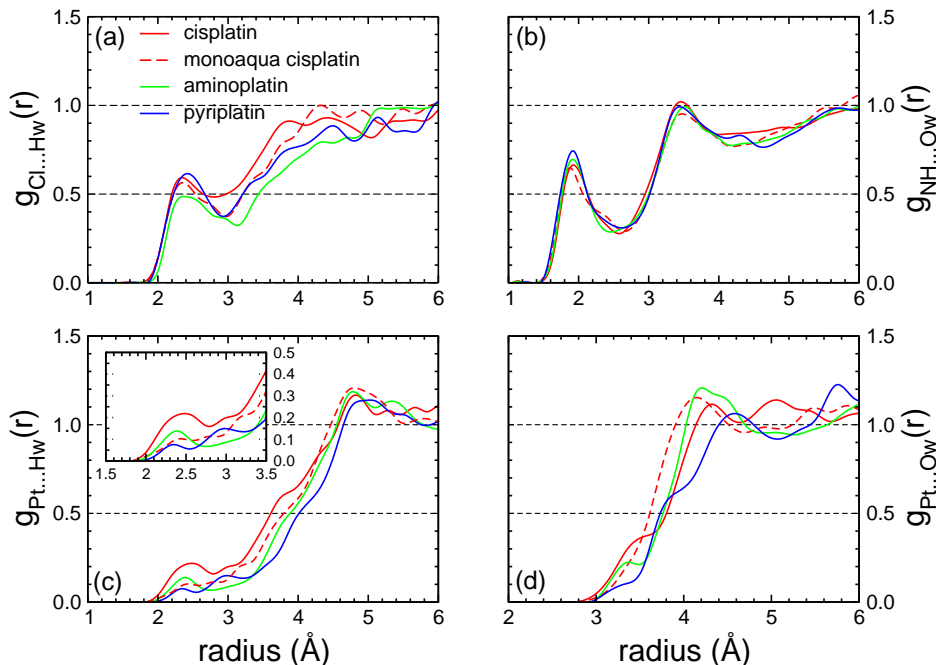As already discussed in Ref. 52 for cisplatin, the $NH\cdots O_w$ $g(r)$ shows that the first and

FIG. 3. Selected $g(r)$ describing the solute-solvent dynamical structures for the solvated bi and monofunctional cisplatin derivatives complexes studied in this work.

TABLE II. Analysis of the ligand–water $g(r)$ calculated for solvated cisplatin and derivatives. The maxima (r_{max}) and the integration radii (r_{int}) are given in Å. The coordination number (n) were evaluated by integrating the corresponding $g(r)$ up to r_{int}. The atoms labeled O_w and H_w refer to water molecules. The $Cl\cdots H_w$ and $NH\cdots O_w$ RDFs are represented on Figures 3(a) and (b), respectively.

Complex	$Pt(NH_3)_2Cl_2$		$[Pt(NH_3)_2(OH_2)Cl]^+$		$[Pt(NH_3)_3Cl]^+$		cis-$[Pt(NH_3)_2(pyridine)Cl]^+$	
Peak[a]	first	second	first	second	first	second	first	second
$Cl\cdots H_w$								
r_{max}	2.3	(3.9/4.4)*	2.3/2.7s	(4.3/4.9)*	2.4/2.9s	(5.1)*	2.4	(4.5/5.1)*
r_{int}^b	2.8	5.0	3.0	5.0	3.1	5.0	2.9	5.0
n	1.8	22.7	2.2	22.6	2.1	19.0	1.9	19.6
$NH\cdots O_w$								
r_{max}	1.9	3.4	1.9/2.4s	3.5	1.9	3.5/3.9s	1.9	3.4/4.3s
r_{int}	2.6	4.5	2.6	4.5	2.5	4.5	2.6	4.5
n	0.7	7.7	0.8	7.6	0.6	7.6	0.6	6.7

[a]Asterisks indicate that the peak(s) is(are) not well resolved. Peak shoulder is indicated by s. [b]For the first integration, r_{int} was fixed to the closest minimum following the first maximum. Beyond these radii fixed values of $r_{int} = 5.0$ and 4.5 Å for the Cl and NH coordination numbers respectively, were considered.

second hydration shells of each NH_3 group integrates around 1 and 8 water molecules, respectively. This also applies to the other platinum complexes (cf. Table II). The fact that the ligand solvation shell is only weakly affected by the variety of ligands bonded to the Pt atom and the charge state of the solute is confirmed by the $Cl\cdots H_w$ $g(r)$ plotted on Figure 3, where each Cl atom integrates in the first neighbor region 2 waters molecules, independently of the system. The second shell is more difficult to discussed due to the

limited resolution of the peaks. Nevertheless, in light of this results, (i) can be directly attributed to the $Cl\cdots H_w$ hydrogen bonds perturbing the $Pt-Cl$ bond strength, whereas (ii) is an indirect consequence of the ammonia group hydration where the preferential arrangement of NH_3 from a static gas-phase optimisation —with one of the hydrogen atom pointing towards the closest Cl lone pair— is lost, relaxing the constraint on the $Cl-Pt-N$ angles of the square planar complexes. Note that, as shown in Table I, a polarizable continuum model (PCM) applied to static isolated solute is able to simulate these two features, demonstrating the concomitant contributions of specific and non-specific solvent effect. In Table III is compared selected structural parameters extracted from the RDFs for cisplatin and the mono-aqua derivative in regard to the previous studies based on DFT-MD.[13,22,30] Even if the results were obtained from different implementations and exchange-correlation functionals —preventing an unbiased comparison— we observe an overall agreement which, besides validating the reliability of our implementation, suggests minor impact of (i) the GGA functional (cf. Ref. 30 DFT-MD simulations performed with BLYP) and (ii) inclusion of the empirical dispersion correction (cf. Ref. 22 ; DFT-MD simulations performed with PBE-D3) on the qualitative description of the ligand first hydration shells.

TABLE III. Comparison of selected structural parameters (in Å) calculated from the ligand–water RDFs of solvated cisplatin obtained from various DFT-MD simulations. See caption and footnotes of Table II for more details.

	$Pt(NH_3)_2Cl_2$				$[Pt(NH_3)_2(OH_2)Cl]^+$		
Method	PBE/BOMD	PBE/CPMD	BLYP/CPMD	PBE+D3/BOMD	PBE/BOMD	BLYP/CPMD	PBE+D3/BOMD
Basis	PAO/NCPP	PW/USPP	PW/NCPP	mixed GTO-PW/NCPP	PAO/NCPP	PW/NCPP	mixed GTO-PW/NCPP
Reference	this work	[13]	[65]	[22]	this work	[65]	[22]
$N\cdots O_w$							
r_{max}	3.0	3.2*	2.9	3.0	2.9	2.9	3.0
r_{int}	3.3	3.4*	–	3.6	3.7	–	3.5
n	2.4	2.5*	2.9	3.6	3.2	3.5	3.5
$NH\cdots O_w$							
r_{max}	1.9	1.9	–	–	1.9/2.4s	–	–
r_{int}	2.6	2.5	–	–	2.6	–	–
n	0.7	0.7	–	–	0.8	–	–
$Cl\cdots O_w$							
r_{max}	3.4*	3.3	3.2*	–	3.5	3.1	–
r_{int}	3.7*	3.7	–	–	3.9	–	–
n	2.8*	2.6	2.9*	–	3.8	3.4	–
$Cl\cdots H_w$							
r_{max}	2.3	2.3	2.3	2.3	2.3/2.7s	2.3	2.3
r_{int}	2.8	2.9	–	2.8	3.0	–	2.9
n	1.8	2.2	1.7	2.2	2.2	2.4	2.2

Another important step in the assessment process of our DFT-MD simulations is to ensure that the characterisitic vibrational modes of the solute and solvent were properly activated. Partial VDOS obtained for cisplatin, aminoplatin and pyriplatin are plotted on Figure 4. As external references, Raman and infra-red theoretical spectra of the isolated molecules are also reported. They were calculated on top of the stationary points obtained at the PBE-GTO-DZP level of theory including a PCM.[63] Here, it is worth to recall that VDOS heights computed from the Fourier transform of the VACFs are not to be compared with spectroscopic intensities, and to emphasize that even if the underlying semiclassical theory involved in evaluating the VDOS —based on the classical propagation of the nuclei on the BO potential energy surface— is quite different from the response function computed from analytic (or numerical) derivatives —based on the harmonic approximation— their comparisons remain valuable for routine checks. As expected, cisplatin and aminoplatin vibrational spectrum are similar in many respects since the Pt center is surrounded by the same type of ligands. In both cases the bond-stretching modes: $N-H$ (> 3200 cm^{-1}),
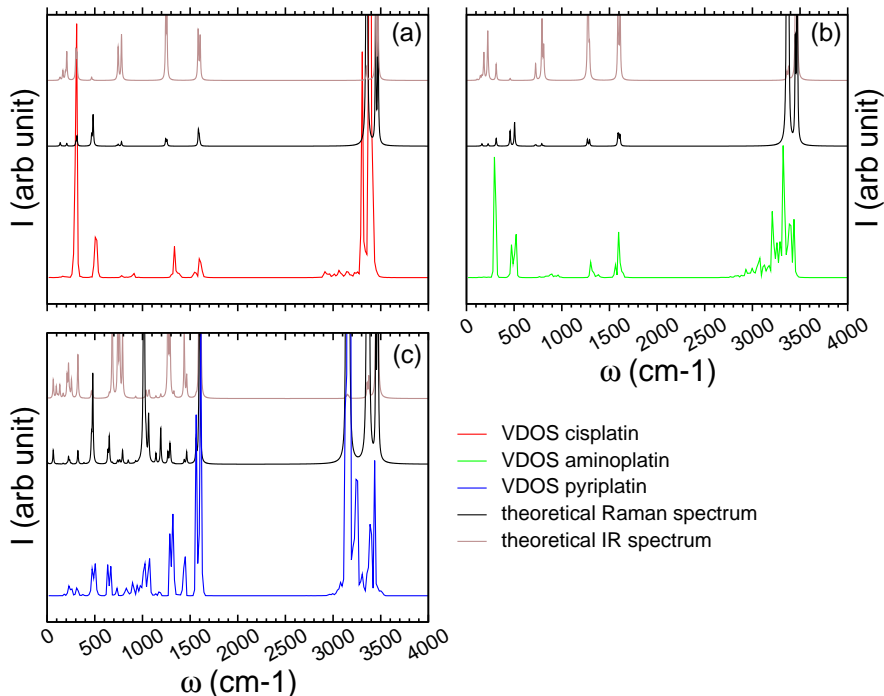
FIG. 4. Comparison between Raman and infra-red theoretical spectra obtained from a molecular approach along with an implicit sovent model and the partial vibrational density of states (VDOS) extracted from the BOMD simulations.

Pt−N ($\sim$ 500 cm^{-1}) and Pt−Cl ($\sim$ 300 cm^{-1}) are observed as well as the NH$_3$ rocking and symmetric/asymetric deformation signatures, found around 800 and 1300/1300 cm^{-1}, respectively.[13,66,67] For pyriplatin, the complexity of the vibrational spectra is increased by the contributions of the pyridine ligand, with the stretching modes: C−H ($\sim$ 3250 cm^{-1}), C−C/C−N (in the range 1100 to 1500 cm^{-1}), the skeletal bending modes along with the out-of-plane C−H wagging ($\sim$ 1000 cm^{-1} and 700 cm^{-1}). As shown on Figure 4, VDOSs extracted for the DFT-BOMD is in fair accordance with the theoretical spectra, such that, given the level of theory PAO-DZP-PBE, we can be confident in the reliability of our simulations when applied to free energy profiles calculation.

B. Inverse hydration

We shall now focussed on the inverse-hydration taking place in the axial region of the square-planar Pt(II) complexes (Scheme 5). It can be observed at the beginning of each MD movies provided in the SI. The hydrogen-like bonding between a water molecule and the metal center following a H-ahead orientation is easily revealed by analysing the $g_{PtO}(r)$ and $g_{PtH}(r)$ available on Figure 3. First we note that for all the systems investigated in this work a non-negligible probability of having a Pt$\cdots$(H$_2$O)$_w$ contact is observed at an intermolecular distance of around 2.4 Å. The poorly-resolved peaks obtained for the Pt$\cdots$H$_w$ (Pt$\cdots$O$_w$) $g(r)$ in the range 2 to 3 (3 to 4) Å illustrate the motion or/and the exchange of H$_2$O with other solvent molecules in close proximity, eg. those available from the Cl hydration shell(s). Another important insight is brought by the height of the peaks, cf. the Pt$\cdots$H$_w$ (Pt$\cdots$O$_w$) $g(r)$ around 2.4 (3.4) Å, indicating a net decrease of the contact occurrence when going from neutral to positively charged complexes. Quantification of the Pt$\cdots$H$_2$O contact is provided in Table IV for the bi- and monofunctional platinum

TABLE IV. Analysis of the Pt–O and Pt–H RDFs calculated for cisplatin and derivatives along with the coordination numbers n ; cf. caption of Table II and Figures 3(c) and (d) for the plots.

Complex	$Pt(NH_3)_2Cl_2$		$[Pt(NH_3)_2(OH_2)Cl]^+$		$[Pt(NH_3)_3Cl]^+$		cis-$[Pt(NH_3)_2(pyridine)Cl]^+$	
Peak	first	second	first	second	first	second	first	second
$Pt\cdots H_w$								
r_{max}	2.5	3.0	2.4	(2.8/3.2)	2.4	na	2.3	(3.0/4.0)
r_{int}	2.6	3.3	2.6	3.3	2.6	3.3	2.6	3.3
n^a	0.5	1.4	0.2	0.9	0.2	0.7	0.1	0.7
$Pt\cdots O_w$								
r_{max}	3.5	4.3	na	4.2	3.4	(4.2/4.5)	3.3	(3.9/4.6)
r_{int}	3.6	4.6	3.6	4.6	3.6	4.6	3.6	4.6
n^a	0.7	6.4	0.7	7.0	0.5	6.7	0.4	5.3

^{a}Since RDFs are poorly-resolved, fixed r_{int} values were considered for the first and second integration.

anticancer drugs, through the evaluation of the Pt(H) and Pt(O) coordination numbers, noted n_{PtH} and n_{PtO}, respectively. Due to the broad shape of the peaks, a set of two integration radius (r_{int} in Table III) were used independently of the complex. For neutral cisplatin, n_{PtH} is evaluated to be within the interval $[0.5, 1.4]$, along with $[0.7, 6.4]$ for n_{PtO}. Note that for larger r_{int}, it is likely that the value of the coordination numbers also incorporate H_2O molecules from the NH_3 and Cl ligand solvent shells. For the set of positively charged complexes, the probability of $Pt\cdots(H_2O)_w$ contact is significantly reduced from $n_{PtH} = [0.2, 0.9]$ for mono-aqua cisplatin to $n_{PtH} = [0.1, 0.7]$ for pyriplatin. For this set, variations of n_{PtO} seems to be more affected by the type of ligand, for which, mono-aqua cisplatin n_{PtO} presents values similar to its neutral parent, whereas for aminoplatin and pyriplatin the coordination number is lowered to $[0.5, 6.7]$ and $[0.4, 5.3]$, respectively. These results corroborate the work of Kroutil et al.[22] which showed, among other findings, that: (i) H_w coordination number decreases with increasing positive charge of the complex, (ii) given a state charge ($+1$ in our case) the H-ahead orientation toward the Pt atom is strongly dependent on the hydrogen bond network formed by the nearby ligands. We refer the reader to this reference for extended discussion on this topic which also includes energetics consideration.
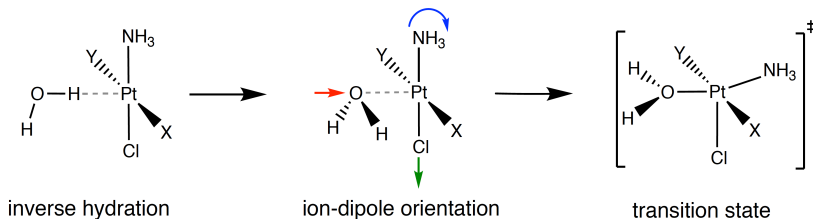
FIG. 5. Structural arrangements of the incoming water molecule at the early stages of the aquation reaction.

Concerning now the second part of this work dealing with evaluation of the hydrolysis free energy profiles of reaction (**1**) and (**2**), among all the water molecules accessible within the solute first solvation shell, it seems quite reasonable to consider the inversely bounded water molecule as the reactant.

C. Hydrolysis free energy profiles

The choice of the reaction coordinate ξ is an important point in BME integration which can be a delicate issue when little is known about the chemical reaction. In this work, we

have relied on the broad (experimental and theoretical) litterature agreeing that cisplatin aquation(s) is a one step process, eg. the S_N2-like mechanism, for which the reactants (R) and products (P) are connected by a single transition state (TS). From this assumption, a rapid analysis of the corresponding saddle point (optimized with a quantum chemistry code) shows that the characteristic imaginary frequency is related to the Cl−Pt−O anti-symmetric stretching mode together with the in-plane rotation of the NH_3 group in trans position (Scheme 5). This led us to consider the difference of distance[68–71] for the reaction coordinate:

$$\xi = ||\mathbf{r}_{Pt} - \mathbf{r}_O|| - ||\mathbf{r}_{Pt} - \mathbf{r}_{Cl}||, \tag{5}$$

where O is the oxygen atom of the H$\cdots$Pt bonded water molecule. Configurations used to initiate the constrained DFT-BOMD trajectories were extracted from the canonical ensemble simulations discussed in Sec. III B. Note that variations of (Helmholtz) free energies as computed from Eq. (1) were directly converted to (Gibbs) free enthalpies since we did not observe any strong variation of pressure during the thermodynamic integration which would have significantly modified the final enthalpy values.
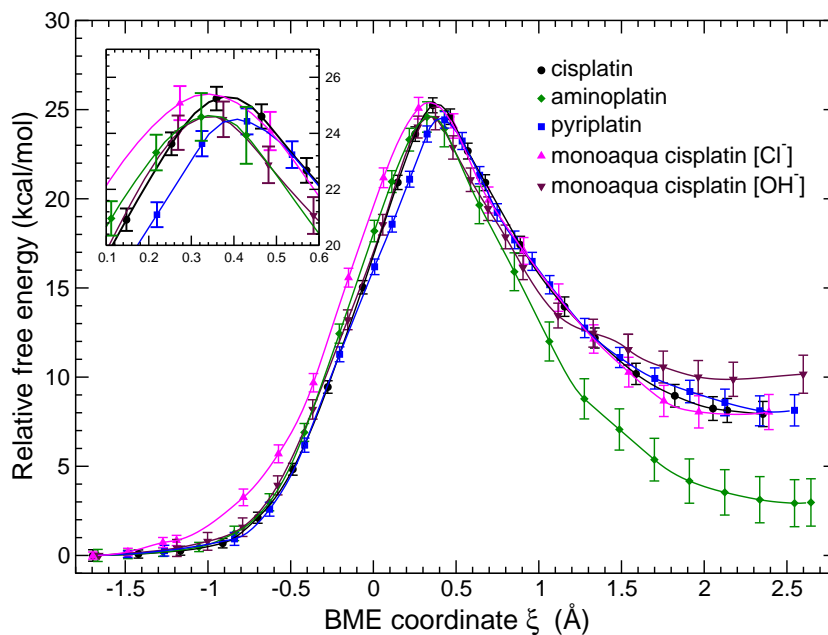
FIG. 6. Free energy path for hydrolysis of cisplatin and derivatives in water at $T = 310$ K using the blue-moon ensemble approach. Curves were interpolated with cubic splines.

Free energy reaction paths are displayed in Figure 6 along with the free enthalpies of activation ($\Delta^{\ddagger}G$) and reaction ($\Delta_r G$) collected in Table V. Concerning the second hydrolysis of cisplatin performed via the monoaqua complex, two set of BME calculation were produced: the first with Cl$^-$ as counterion following the first hydrolysis (later abbreviated by monoaqua[Cl]), the second from afresh NVT equilibration in which Cl$^-$ has been replaced by OH$^-$ (abbreviated by monoaqua[OH]). From Figure 6 we observe very similar energy profiles from the attack of the water molecule up to the transitions states. Evaluated $\Delta^{\ddagger}G$ for cationic monofuntional species are found to be lower of about 1 kcal $\cdot$ mol^{-1} than the reference value of 25 kcal $\cdot$ mol^{-1} obtained for the neutral parent. The presence of the Cl$^-$ counterion during the second hydrolysis of cisplatin tends to slightly decrease the barrier, but without dramatic effect. Indeed, major deviations between aquation profiles are found after the TS. This lead to noticeable differences in the values of $\Delta_r G$, for which we found that the aminoplatin aquation is endothermic by 3 kcal $\cdot$ mol^{-1} compared to 8 for cisplatin,

pyriplatin and moaqua[Cl], whereas for moaqua[OH] the free enthalpy of reaction reach the value of 10 kcal·mol^{-1}. It is tempting to compare these values to available experimental data. This should be done with lots of care owing to: (i) the large amount of papers dealing with this subject, which comes generally with the same amount of differences in experimental condition, (ii) the limitations of our model in reproducing these conditions. As a result,

Reactant	Counterion	$\Delta^{\ddagger}G$ (kcal·mol^{-1})	$\Delta_r G$ (kcal·mol^{-1})
cisplatin	none	25.3 ± 0.4	7.9 ± 0.7
mono-aqua cisplatin	OH^{-}	25.4 ± 0.6	10.2 ± 1.1
	Cl^{-}	24.5 ± 0.6	8.0 ± 1.0
aminoplatin	OH^{-}	24.5 ± 0.8	2.9 ± 1.3
pyriplatin	OH^{-}	24.4 ± 0.5	8.1 ± 0.9

TABLE V. Free enthalpies of activations and reactions for aquation of cisplatin and derivatives in water at $T = 310$ K using the blue-moon ensemble approach.

even if the pH of the aqueous media can impact significantly the kinetic of the reactions —as shown in the comprehensive study of House and coworkers[72–74]— we must emphasize that the precision reach by the BME simulations remains far from the chemical accuracy required to discuss variation in activation energies below 1 kcal·mol^{-1}.[?] From Refs. 72,73,75–79 we can establish a consensus on the experimental free enthalpy (at ambient temperature) for both, the first and second aquation, to be between 23 and 24 kcal·mol^{-1}. The experimental values for the cationic aminoplatin and pyriplatin are expected to be within this range.[40] A consensus on the endothermic property of the aquation reactions can also be drawn, with $\Delta_r G$ for cisplatin experimentally evaluated to be in the range 3-10 kcal·mol^{-1}.[72,73,78] Our results which are in line with experimental data should not be overinterpreted. Whereas we are quite confident in the reliability of the computed BME activation enthalpies, the thermodynamic quantities must not be considered as definitive. The limited size of cell can not prevent intramolecular ion pair contact to occur (the outermost Cl$\cdots$Pt distance being of 6.5 Å). For aminoplatin, the larger error bars on the integrated free energy observed at the late stages of the reaction suggest that the final $\Delta_r G$ is not fully converged.

In order to gain some insights into the reactants motion and solvent reorganisation along the reaction path, visual inspection of the constrained MD movies is quite instructive. Representative examples are provided in the SI for cisplatin and pyriplatin. For all the complexes investigated similar trends in the evolution of skeletal bond parameters and solvent shell relative to the reactant constrained dynamics were found. The study cases of cisplatin and pyriplatin aquations are depicted in Figures 7 and 8, where the variation of selected structural parameters are plotted as a function of ξ. At the beginning of the reaction ($\xi < 0$), the square planar structure with the inverse-hydration is globally conserved in both cases. In this regime, for cisplatin, the net decrease of the Pt$\cdots$O bond length ($d_{\mathrm{PtO}} = 3.8 \rightarrow 2.7$ Å) is accompanied by a weaker increase of the Pt$\cdots$Cl distance ($d_{\mathrm{PtCl}} = 2.4 \rightarrow 2.7$ Å) whereas the N$-$Pt$-$O (α), O$-$Pt$-$Cl (β) and Cl$-$Pt$-$N (γ) angles oscillate around mean values of 100, 85 and 175°, respectively. These observations also hold for pyriplatin with slight differences in values. For cisplatin, magnitude of the variations along ξ observed for α and β, which are much higher than for γ, indicates that the constrained water molecule remains free to visit the axial region of the square-planar complex. It seems to be less pronounced for pyriplatin. The difference in lability of the inversely bonded H$_2$O between the two complexes is apparent when comparing the standard deviation (std) of the Pt$\cdots$H distances plotted on Figure 8. For cisplatin we occasionally observe that these distances collapse towards a single value, eg. at $\xi = (-1.2, -0.5)$, indicating H-atom swap through the rotation along the axis perpendicular to the H$_2$O molecular plan. The variations of the H$-$O$-$Pt angles (θ_1, θ_2) with mean values of about $(20, 100) \pm 20°$ for cisplatin, and $(10, 110) \pm 5°$ for pyriplatin confirm the preferential inverse-hydration orientation, and for the later case, the reduced mobility of the H$_2$O-reactant.

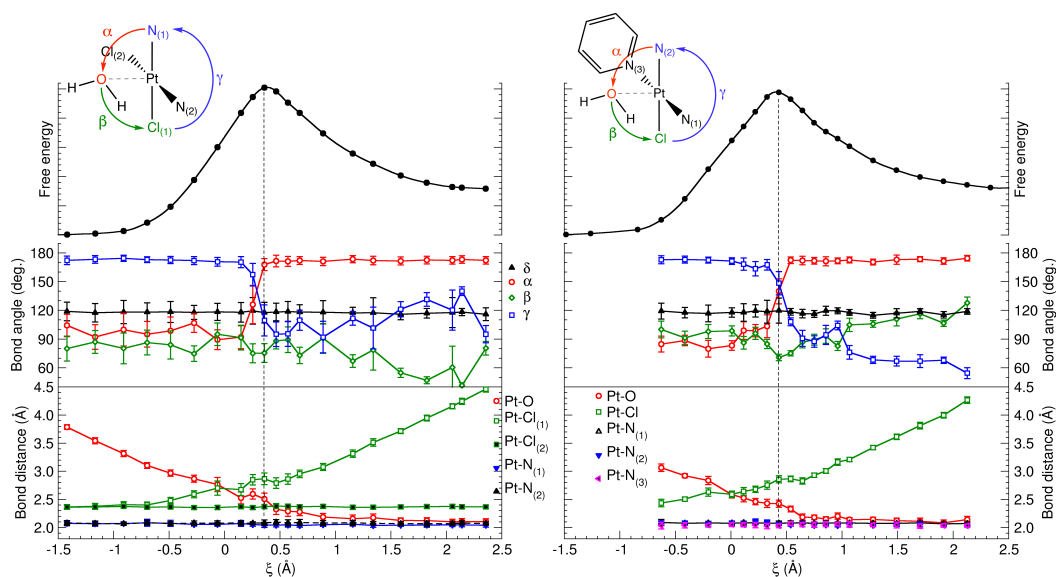When approaching the transition state located at $\xi = 0.36$ and 0.43 Å for cisplatin and

FIG. 7. Ensemble average of the skeletal bond angles and distances as a function of the BME coordinate obtained for cisplatin (left) and pyriplatin (right) aquation. Vertical bars correspond to the standard deviations. Free energy profile along the reaction path has been included to guide the eye.

pyriplatin respectively, the inversely bonded H_2O is activated *via* the ion-dipole orientation depicted in Scheme 5 with $d_{PtO} \simeq 2.5$ and $d_{PtH} \simeq 3.0$ Å. For cisplatin, when $\xi > 0.1$ ($\xi > 0.3$ for pyriplatin), the rotation of the NH_3 group is engaged leading to the TS. Note that, within the TS region, reported $Pt\cdots H$ distances and angles are weakly affected compared to the rotation angles (α, γ). By identifying on Figure 7 the skeletal parameters corresponding to the maximum of free energy, it seems that the cisplatin TS is closer to a square pyramidal structure than a trigonal bipyramid as observed in gas phase calculations.[28] With $\alpha \simeq \gamma \simeq 140°$ a trigonal pyramid can be clearly assigned to pyriplatin. For $\xi > 0.9$, the water molecule is fully coordinated to the metal center with a typical bond length $d_{PtO} \simeq 2.1$ Å, and the Cl anion is released to bulk water. Inspection of the cisplatin BME integration movie at $\xi = 1.15$ reveals that the singularity on Figure 8 is due to the departure of one of the H_2O-ligand proton towards the solvent shell. From Figure 7, looking to the $Pt-N$ and unconstrained $Pt-Cl$ mean bond lengths, it is interesting to outline that the corresponding ligands are spectator of the reaction in agreement with the in-plane symmetry of the transition state. This is well exemplified by the mean angle $\delta = (\alpha + \beta + \gamma)/3$ which remains fixed to 120° with standard deviation not exceeding 10° for both cases, showing that there are only weak perturbations from outside the $N-O-Cl$ plane.

By visualizing the constrained MD trajectories reported in the SI, it is rather clear that the activated water molecule is embedded in a hydrogen-bond network throughout the whole course of the aquation reaction. To quantify the number of first nearest neighbor solvent molecules surrounding the H_2O-reactant and Cl-product, the coordination numbers n_{OO_w}, (n_{OH_w}, n_{HO_w}) and n_{ClH_w} are plotted on Figure 8 as a function of ξ. They were evaluated from the ensemble averages (cf. Sec. II B) by integrating the corresponding RDFs up to standard radii[51,80] of 3.2, 2.5 and 2.9 Å, respectively. Even if at first sight the evolution of n is somewhat erratic due to the short time sampling, we can extract some relevant trends. At the beginning of the reaction, the inversely bonded water molecule integrates around 3 solvent molecules respecting its H-bond donor[1]/acceptor[2] capacity. Around the ion-dipole orientation region, as expected, H-bond acceptor (donor) capacity of the H_2O-reactant reduces (raises). At the transition state, around 2 and 1 solvent molecule(s) are in close proximity of the activated H_2O in cisplatin and pyriplatin, respectively. After this
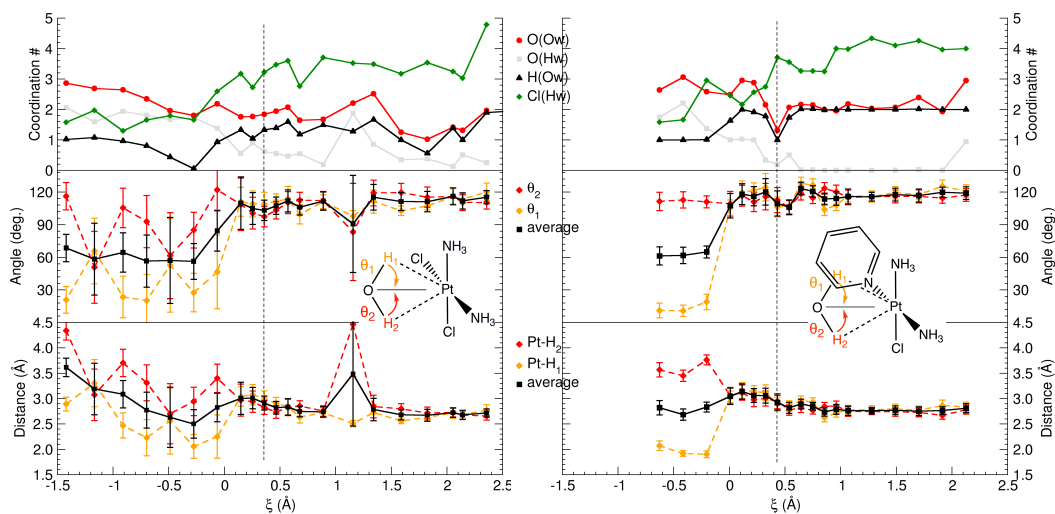
FIG. 8. Ensemble average of selected geometrical parameters describing the attack of inversely bonded water molecule for cisplatin (left) and pyriplatin (right) aquation reaction. See also the caption of Figure 7. Coordination numbers reported on the upper panel were evaluated from the RDFs.

step, the average number acceptor-type H-bond continue to diminish whereas donor-type stabilizes to 2. The evolution of the H_2O-reactant H-bond network contrasts with the global increase of the solvent shell size surrounding the Cl-product. Due the limited size of the model n_{ClH_w} never really stabilized to the reference value comprised between 5 and 6 as obtained for free solvated chlorine anion.[80]

Finally, the BME aquation profiles and their analysis suggest that the aquation reaction of cisplatin and its monofunctional derivatives presenting a Cl-leaving group is likely to be independent of the charge state the type and number of N-donor ligands despite variations in the mobility and microsolvation of the activated water molecule. Even if conditioned by the choice of coordinate, the inverse hydration followed by the ion-dipole orientation seems to be a prerequisite to reach the transition state.

IV. CONCLUSION AND OUTLOOK

In this work, reliable DFT-MD simulations of the aquation process of cisplatin and a set of monofunctional platinum anticancer drugs have been performed using constrained dynamics in conjunction with BME thermodynamic integration. Given the level of theory, accuracy of about 1 kcal · mol^{-1} has been reached on the activation barrier. For the set of square-planar Pt(II) complexes, it is found that the kinetic of the reaction is independent of the ligands and the charge state. It seems that the free enthalpies of reaction differ from a few kcal · mol^{-1} from one complex to another, and counterions can impact the thermodynamic quantity with variations in the same range of magnitude. This result need to be confirmed by performing larger scale DFT-MD simulations. We conclude that it is likely that the mono and bifunctional platinum anticancer drugs behave the same way during the time lapse between the cellular uptake and the DNA platination.

From a computational point of view, such kind of approach alleviates many intricacies related to modelling chemical reactions in aqueous solvent which are commonly based on isolated molecule approximation where thermodynamic quantities are computed from the ideal gas approximation. Even if the protocol used here is computationally expensive, we believe that it will become a routine task in near future along with the possibility of increasing the system size and using more sophisticated exchange correlation functionals,

especially with the Conquest code which have been developped to perform large scale DFT simulations. This work opens the way for futur high level theoretical investigations of the anticancer activity of monofuntional platinum complexes which are important steps for approaching *in silico* design of new potent drugs.

[1] Wheate, N. J.; Walker, S.; Craig, G. E.; Oun, R. The status of platinum anticancer drugs in the clinic and in clinical trials. *Dalton Trans.* **2010**, *39*, 8113–8127.

[2] Johnstone, T. C.; Park, G. Y.; Lippard, S. J. Understanding and Improving Platinum Anticancer Drugs – Phenanthriplatin. *Anticancer Res.* **2014**, *34*, 471–476.

[3] Apps, M. G.; Choi, E. H. Y.; Wheate, N. J. The state-of-play and future of platinum drugs. *Endocr. Relat. Cancer* **2015**, *22*, R219–R233.

[4] Johnstone, T. C.; Suntharalingam, K.; Lippard, S. J. The Next Generation of Platinum Drugs: Targeted Pt(II) Agents, Nanoparticle Delivery, and Pt(IV) Prodrugs. *Chem. Rev.* **2016**, *116*, 3436–3486.

[5] Brabec, V.; Kasparkova, J. Modifications of DNA by platinum complexes. *Drug Resistance Updates* **2005**, *8*, 131–146.

[6] Chabner, B. A.; Roberts, T. G. Chemotherapy and the war on cancer. *Nat. Rev. Cancer* **2005**, *5*, 65–72.

[7] Kelland, L. The resurgence of platinum-based cancer chemotherapy. *Nat. Rev. Cancer* **2007**, *7*, 573–584.

[8] Hambley, T. W. The influence of structure on the activity and toxicity of Pt anti-cancer drugs. *Coord. Chem. Rev.* **1997**, *166*, 181–223.

[9] Ziegler, C. J.; Silverman, A. P.; Lippard, S. J. High-throughput synthesis and screening of platinum drug candidates. *J. Biol. Inorg. Chem.* **2000**, *5*, 774–783.

[10] Jamieson, E. R.; Lippard, S. J. Structure, Recognition, and Processing of Cisplatin-DNA Adducts. *Chem. Rev.* **1999**, *99*, 2467–2498.

[11] Dhar, S.; Lippard, S. J. In *Platinum and Other Heavy Metal Compounds in Cancer Chemotherapy*; Bonetti, A., Leone, R., Muggia, F. M., Howell, S. B., Eds.; Cancer Drug Discovery and Development; Humana Press, 2009; pp 135–147.

[12] Vidossich, P.; Lledós, A.; Ujaque, G. First-Principles Molecular Dynamics Studies of Organometallic Complexes and Homogeneous Catalytic Processes. *Acc. Chem. Res.* **2016**, *49*, 1271–1278; (a) Beret, E. C.; Martínez, J. M.; Pappalardo, R. R.; Sánchez Marcos, E.; Doltsinis, N. L.; Marx, D. Explaining Asymmetric Solvation of Pt(II) versus Pd(II) in Aqueous Solution Revealed by Ab Initio Molecular Dynamics Simulations. *J. Chem. Theory Comput.* **2008**, *4*, 2108–2121; (b) Beret, E. C.; Pappalardo, R. R.; Marx, D.; Sánchez Marcos, E. Characterizing Pt-Derived Anticancer Drugs from First Principles: The Case of Oxaliplatin in Aqueous Solution. *ChemPhysChem* **2009**, *10*, 1044–1052; (c) Vidossich, P.; Ortuño, M. Á.; Ujaque, G.; Lledós, A. Do Metal...Water Hydrogen Bonds Hold in Solution? Insight from Ab Initio Molecular Dynamics Simulations. *ChemPhysChem* **2011**, *12*, 1666–1668.

[13] Truflandier, L. A.; Sutter, K.; Autschbach, J. Solvent Effects and Dynamic Averaging of ^{195}Pt NMR Shielding in Cisplatin Derivatives. *Inorg. Chem.* **2011**, *50*, 1723–1732.

[14] Sutter, K.; Truflandier, L. A.; Autschbach, J. NMR J-Coupling Constants in Cisplatin Derivatives Studied by Molecular Dynamics and Relativistic DFT. *ChemPhysChem* **2011**, *12*, 1448–1455.

[15] Baidina, I. A.; Podberezskaya, N. V.; Krylova, L. F.; Borisov, S. V. Crystal structure of trans-dichloroammineglycineplatinum (II) monohydrate trans-[PtNH$_3$(H$_2$NCH$_2$COOH)Cl$_2$]·H$_2$O. *J. Struct. Chem.* **1981**, *22*, 463–465.

[16] Rizzato, S.; Bergès, J.; Mason, S. A.; Albinati, A.; Kozelka, J. Dispersion-Driven Hydrogen Bonding: Predicted Hydrogen Bond between Water and Platinum(II) Identified by Neutron Diffraction. *Angew. Chem. Int. Ed.* **2010**, *49*, 7440–7443.

[17] Kozelka, J.; Bergès, J.; Attias, R.; Fraitag, J. Hydrogen Bond with a Strong Dispersion Component. *Angew. Chem. Int. Ed.* **2000**, *39*, 198–201.

[18] Lopes, J. F.; Rocha, W. R.; Dos Santos, H. F.; De Almeida, W. B. Theoretical study of the potential energy surface for the interaction of cisplatin and their aquated species with water. *J. Chem. Phys.* **2008**, *128*, 165103–14.

[19] Aono, S.; Mori, T.; Sakaki, S. 3D-RISM-MP2 Approach to Hydration Structure of Pt(II) and Pd(II) Complexes: Unusual H-Ahead Mode vs Usual O-Ahead One. *J. Chem. Theory Comput.* **2016**, *12*, 1189–1206.

[20] Bergès, J.; Fourré, I.; Pilmé, J.; Kozelka, J. Quantum Chemical Topology Study of the Water-Platinum(II) Interaction. *Inorg. Chem.* **2013**, *52*, 1217–1227.

[21] Melchior, A.; Tolazzi, M.; Martínez, J. M.; Pappalardo, R. R.; Sánchez Marcos, E. Hydration of Two Cisplatin Aqua-Derivatives Studied by Quantum Mechanics and Molecular Dynamics Simulations. *J. Chem. Theory Comput.* **2015**, *11*, 1735–1744.

[22] Kroutil, O.; Předota, M.; Chval, Z. Pt···H Nonclassical Interaction in Water-Dissolved Pt(II) Complexes: Coaction of Electronic Effects with Solvent-Assisted Stabilization. *Inorg. Chem.* **2016**, *55*, 3252–3264.

[23] Bancroft, D. P.; Lepre, C. A.; Lippard, S. J. Platinum-195 NMR kinetic and mechanistic studies of cis- and trans-diamminedichloroplatinum(II) binding to DNA. *J. Am. Chem. Soc.* **1990**, *112*, 6860–6871.

[24] Knox, R. J.; Friedlos, F.; Lydall, D. A.; Roberts, J. J. Mechanism of Cytotoxicity of Anticancer Platinum Drugs: Evidence That cis-Diamminedichloroplatinum(II) and cis-Diammine-(1,1-cyclobutanedicarboxylato)platinum(II) Differ Only in the Kinetics of Their Interaction with DNA. *Cancer Res.* **1986**, *46*, 1972–1979.

[25] Alberts, D. S.; Dorr, R. T. New Perspectives on an Old Friend: Optimizing Carboplatin for the Treatment of Solid Tumors. *The Oncologist* **1998**, *3*, 15–34.

[26] Johnstone, T. C.; Alexander, S. M.; Wilson, J. J.; Lippard, S. J. Oxidative halogenation of cisplatin and carboplatin: synthesis, spectroscopy, and crystal and molecular structures of Pt(IV) prodrugs. *Dalton Trans.* **2014**, *44*, 119–129.

[27] Blommaert, F. A.; van Dijk-Knijnenburg, H. C. M.; Dijt, F. J.; den Engelse, L.; Baan, R. A.; Berends, F.; Fichtinger-Schepman, A. M. J. Formation of DNA Adducts by the Anticancer Drug Carboplatin: Different Nucleotide Sequence Preferences in Vitro and in Cells. *Biochemistry* **1995**, *34*, 8474–8480.

[28] Zhang, Y.; Guo, Z.; You, X. Hydrolysis Theory for Cisplatin and Its Analogues Based on Density Functional Studies. *J. Am. Chem. Soc.* **2001**, *123*, 9378–9387; (a) Robertazzi, A.; Platts, J. A. Hydrogen bonding, solvation, and hydrolysis of cisplatin: A theoretical study. *J. Comput. Chem.* **2004**, *25*, 1060–1067; (b) Lau, J. K.; Deubel, D. V. Hydrolysis of the Anticancer Drug Cisplatin: Pitfalls in the Interpretation of Quantum Chemical Calculations. *J. Chem. Theory Comput.* **2006**, *2*, 103–106; (c) Alberto, M. E.; Lucas, M. F. A.; Pavelka, M.; Russo, N. The Second-Generation Anticancer Drug Nedaplatin: A Theoretical Investigation on the Hydrolysis Mechanism. *J. Phys. Chem. B* **2009**, *113*, 14473–14479; (d) Lucas, M. F. A.; Pavelka, M.; Alberto, M. E.; Russo, N. Neutral and Acidic Hydrolysis Reactions of the Third Generation Anticancer Drug Oxaliplatin. *J. Phys. Chem. B* **2009**, *113*, 831–838; (e) Banerjee, S.; Sengupta, P. S.; Mukherjee, A. K. Trans Platinum Anticancer Drug AMD443: A Detailed Theoretical Study by DFT-TST Method on the Hydrolysis Mechanism. *Chem. Phys. Lett.* **2010**, *487*, 108–115; (f) Melchior, A.; Marcos, E. S.; Pappalardo, R. R.; Martínez, J. M. Comparative study of the hydrolysis of a third- and a first-generation platinum anticancer complexes. *Theor. Chem. Acc.* **2010**, *128*, 627–638.

[29] Carloni, P.; Sprik, M.; Andreoni, W. Key Steps of the cis-Platin-DNA Interaction: Density Functional Theory-Based Molecular Dynamics Simulations. *J. Phys. Chem. B* **2000**, *104*, 823–835.

[30] Lau, J. K.-C.; Ensing, B. Hydrolysis of cisplatin—a first-principles metadynamics study. *Phys. Chem. Chem. Phys.* **2010**, *12*, 10348–10355.

[31] Yokogawa, D.; Sato, H.; Sakaki, S. New generation of the reference interaction site model self-consistent field method: Introduction of spatial electron density distribution to the solvation theory. *J. Chem. Phys.* **2007**, *126*, 244504.

[32] Yokogawa, D.; Sato, H.; Sakaki, S. Analytical energy gradient for reference interaction site model self-consistent field explicitly including spatial electron density distribution. *J. Chem. Phys.* **2009**, *131*, 214504.

[33] Yokogawa, D.; Ono, K.; Sato, H.; Sakaki, S. Theoretical study on aquation reaction of cis-platin complex: RISM–SCF–SEDD, a hybrid approach of accurate quantum chemical method and statistical mechanics. *Dalton Trans.* **2011**, *40*, 11125–11130.

[34] Hollis, L. S.; Amundsen, A. R.; Stern, E. W. Chemical and biological properties of a new series of cis-diammineplatinum(II) antitumor agents containing three nitrogen donors: cis-[Pt(NH$_3$)$_2$(N-donor) Cl]$^+$. *J. Med. Chem.* **1989**, *32*, 128–136.

[35] Brabec, V. DNA Modifications by antitumor platinum and ruthenium compounds: Their recognition and repair. *Prog. Nucleic Acid Res. Mol. Biol.* **2002**, *71*, 1–68.

[36] Bursova, V.; Kasparkova, J.; Hofr, C.; Brabec, V. Effects of Monofunctional Adducts of Platinum(II) Complexes on Thermodynamic Stability and Energetics of DNA Duplexes. *Biophys. J.* **2005**, *88*, 1207–1214.

[37] Lovejoy, K. S.; Todd, R. C.; Zhang, S.; McCormick, M. S.; D'Aquino, J. A.; Reardon, J. T.; Sancar, A.; Giacomini, K. M.; Lippard, S. J. cis-Diammine(pyridine)chloroplatinum(II), a monofunctional platinum(II) antitumor agent: Uptake, structure, function, and prospects. *PNAS* **2008**, *105*, 8902–8907.

[38] Wang, D.; Zhu, G.; Huang, X.; Lippard, S. J. X-ray structure and mechanism of RNA polymerase II stalled at an antineoplastic monofunctional platinum-DNA adduct. *PNAS* **2010**, *107*, 9584–9589.

[39] Zhu, G.; Myint, M.; Ang, W. H.; Song, L.; Lippard, S. J. Monofunctional Platinum–DNA Adducts Are Strong Inhibitors of Transcription and Substrates for Nucleotide Excision Repair in Live Mammalian Cells. *Cancer Res.* **2012**, *72*, 790–800.

[40] Park, G. Y.; Wilson, J. J.; Song, Y.; Lippard, S. J. Phenanthriplatin, a monofunctional DNA-binding platinum anticancer drug candidate with unusual potency and cellular activity profile. *PNAS* **2012**, *109*, 11987–11992.

[41] Johnstone, T. C.; Alexander, S. M.; Lin, W.; Lippard, S. J. Effects of Monofunctional Platinum Agents on Bacterial Growth: A Retrospective Study. *J. Am. Chem. Soc.* **2014**, *136*, 116–118.

[42] Bowler, D. R.; Choudhury, R.; Gillan, M. J.; Miyazaki, T. Recent progress with large-scale ab initio calculations: the CONQUEST code. *phys. stat. sol. (b)* **2006**, *243*, 989–1000.

[43] Bowler, D. R.; Miyazaki, T. Calculations for millions of atoms with density functional theory: linear scaling shows its potential. *J. Phys.: Condens. Matter* **2010**, *22*, 074207.

[44] Hernández, E.; Gillan, M. J.; Goringe, C. M. Linear-scaling density-functional-theory technique: The density-matrix approach. *Phys. Rev. B* **1996**, *53*, 7147.

[45] Sankey, O. F.; Niklewski, D. J. Ab initio multicenter tight-binding model for molecular-dynamics simulations and other applications in covalent systems. *Phys. Rev. B* **1989**, *40*, 3979–3995.

[46] Junquera, J.; Paz, Ó.; Sánchez-Portal, D.; Artacho, E. Numerical atomic orbitals for linear-scaling calculations. *Phys. Rev. B* **2001**, *64*, 235111.

[47] Torralba, A. S.; Todorović, M.; Brázdová, V.; Choudhury, R.; Miyazaki, T.; Gillan, M. J.; Bowler, D. R. Pseudo-atomic orbitals as basis sets for the O(N) DFT code CONQUEST. *J. Phys.: Condens. Matter*

2008, *20*, 294206.

[48] Troullier, N.; Martins, J. L. Efficient pseudopotentials for plane-wave calculations. *Phys. Rev. B* **1991**, *43*, 1993–2006.

[49] Perdew, J. P.; Burke, K.; Ernzerhof, M. Generalized Gradient Approximation Made Simple. *Phys. Rev. Lett.* **1996**, *77*, 3865–3868.

[50] Lin, I.-C.; Seitsonen, A. P.; Tavernelli, I.; Rothlisberger, U. Structure and Dynamics of Liquid Water from ab Initio Molecular Dynamics—Comparison of BLYP, PBE, and revPBE Density Functionals with and without van der Waals Corrections. *J. Chem. Theory Comput.* **2012**, *8*, 3902–3910.

[51] DiStasio, R. A.; Santra, B.; Li, Z.; Wu, X.; Car, R. The individual and collective effects of exact exchange and dispersion interactions on the ab initio structure of liquid water. *J. Chem. Phys.* **2014**, *141*, 084502.

[52] Truflandier, L. A.; Autschbach, J. Probing the Solvent Shell with 195Pt Chemical Shifts: Density Functional Theory Molecular Dynamics Study of Pt(II) and Pt(IV) Anionic Complexes in Aqueous Solution. *J. Am. Chem. Soc.* **2010**, *132*, 3472–3483.

[53] Verlet, L. Computer ”Experiments” on Classical Fluids. I. Thermodynamical Properties of Lennard-Jones Molecules. *Phys. Rev.* **1967**, *159*, 98–103.

[54] Martyna, G. J.; Klein, M. L.; Tuckerman, M. Nosé–Hoover chains: The canonical ensemble via continuous dynamics. *J. Chem. Phys.* **1992**, *97*, 2635–2643.

[55] Hirakawa, T.; Suzuki, T.; Bowler, D. R.; Miyazaki, T. Canonical-ensemble extended Lagrangian Born–Oppenheimer molecular dynamics for the linear scaling density functional theory. *J. Phys.: Condens. Matter* **2017**, *29*, 405901.

[56] Carter, E.; Ciccotti, G.; Hynes, J. T.; Kapral, R. Constrained reaction coordinate dynamics for the simulation of rare events. *Chem. Phys. Lett.* **1989**, *156*, 472–477.

[57] Sprik, M.; Ciccotti, G. Free energy from constrained molecular dynamics. *J. Chem. Phys.* **1998**, *109*, 7737–7744.

[58] Ryckaert, J.-P.; Ciccotti, G.; Berendsen, H. J. Numerical integration of the cartesian equations of motion of a system with constraints: molecular dynamics of n-alkanes. *J. Comput. Phys.* **1977**, *23*, 327–341.

[59] Andersen, H. C. Rattle: A "velocity" version of the shake algorithm for molecular dynamics calculations. *J. Comput. Phys.* **1983**, *52*, 24–34.

[60] Ciccotti, G.; Ryckaert, J.-P. Molecular dynamics simulation of rigid molecules. *Comp. Phys. Rep.* **1986**, *4*, 346–392.

[61] Jacucci, G.; Rahman, A. Comparing the efficiency of Metropolis Monte Carlo and molecular-dynamics methods for configuration space sampling. *Il Nuovo Cimento D* **1984**, *4*, 341–356.

[62] Giannozzi, P.; et al., *J. Phys.: Condens. Matter* **2009**, *21*, 395502.

[63] Frisch, M. J.; et al., Gaussian09. *Gaussian 09, Revision A.02;* Gaussian, Inc., Wallingford, CT, 2009

[64] Press, W. H.; Flannery, B. P.; Teukolsky, S. A.; Vetterling, W. T. *Numerical Recipes in Fortran 77: The Art of Scientific Computing*, 2nd ed.; Cambridge University Press: Cambridge England ; New York, NY, USA, 1992.

[65] Lau, J. K.; Ensing, B. Hydrolysis of cisplatina first-principles metadynamics study. *Phys. Chem. Chem. Phys.* **2010**,

[66] Nakamoto, K.; McCarthy, P. J.; Fujita, J.; Condrate, R. A.; Behnke, G. T. Infrared Studies of Ligand-Ligand Interaction in Dihalogenodiammineplatinum(II) Complexes. *Inorg. Chem.* **1965**, *4*, 36–43.

[67] Wysokiński, R.; Michalska, D. The performance of different density functional methods in the calculation of molecular structures and vibrational spectra of platinum(II) antitumor drugs: cisplatin and carboplatin. *J. Comput. Chem.* **2001**, *22*, 901–912.

[68] Raugei, S.; Cardini, G.; Schettino, V. An *ab initio* molecular dynamics study of the SN$_2$ reaction Cl$^-$+CH$_3$Br→CH$_3$Cl+Br$^-$. *The Journal of Chemical Physics* **1999**, *111*, 10887–10894.

[69] Yang, S.-Y.; Fleurat-Lessard, P.; Hristov, I.; Ziegler, T. Free Energy Profiles for the Identity SN2 Reactions Cl$^-$ + CH$_3$Cl and NH$_3$ + H$_3$BNH$_3$: A Constraint Ab Initio Molecular Dynamics Study. *J. Phys. Chem. A* **2004**, *108*, 9461–9468.

[70] Bühl, M.; Kabrede, H. Mechanism of Water Exchange in Aqueous Uranyl(VI) Ion. A Density Functional Molecular Dynamics Study. *Inorg. Chem.* **2006**, *45*, 3834–3836.

[71] Komeiji, Y.; Ishikawa, T.; Mochizuki, Y.; Yamataka, H.; Nakano, T. Fragment Molecular Orbital method-based Molecular Dynamics (FMO-MD) as a simulator for chemical reactions in explicit solvation. *J. Comput. Chem.* **2009**, *30*, 40–50.

[72] Miller, S. E.; House, D. A. The hydrolysis products of cis-diamminedichloroplatinum(II). 1. The kinetics of formation and anation of the cis-diammine(aqua)chloroplatinum(II) cation in acidic aqueous solution. *Inorg. Chim. Acta* **1989**, *161*, 131–137.

[73] Miller, S. E.; House, D. A. The hydrolysis products of cis-dichlorodiammineplatinum(II) 2. The kinetics of formation and anation of the cis-diamminedi(aqua)platinum(II) cation. *Inorg. Chim. Acta* **1989**, *166*, 189–197.

[74] Miller, S. E.; House, D. A. The hydrolysis products of cis-dichlorodiammineplatinum(II) 3. Hydrolysis kinetics at physiological pH. *Inorg. Chim. Acta* **1990**, *173*, 53–60.

[75] Reishus, J. W.; Martin, D. S. cis-Dichlorodiammineplatinum(II). Acid Hydrolysis and Isotopic Exchange of the Chloride Ligands. *J. Am. Chem. Soc.* **1961**, *83*, 2457–2462.

[76] Marti, N.; Bon Hoa, G. H.; Kozelka, J. Reversible hydrolysis of [PtCl(dien)]$^+$ and [PtCl(NH$_3$)$_3$]$^+$. Determination of the rate constants using UV spectrophotometry. *Inorg. Chem. Comm.* **1998**, *1*, 439–442.

[77] Davies, M. S.; Berners-Price, S. J.; Hambley, T. W. Slowing of Cisplatin Aquation in the Presence of

DNA but Not in the Presence of Phosphate: Improved Understanding of Sequence Selectivity and the Roles of Monoaquated and Diaquated Species in the Binding of Cisplatin to DNA. *Inorg. Chem.* **2000**, *39*, 5603–5613.

[78] Lee, K. W.; Martin, D. S. Cis-dichlorodiammineplatinum(II). Aquation equilibria and isotopic exchange of chloride ligands with free chloride and tetrachloroplatinate(II). *Inorg. Chim. Acta* **1976**, *17*, 105–110.

[79] Vinje, J.; Sletten, E.; Kozelka, J. Influence of dT_{20} and $[d(AT)_{10}]_2$ on Cisplatin Hydrolysis Studied by Two-Dimensional [^{1}H,^{15}N] HMQC NMR Spectroscopy. *Chem. Eur. J.* **2005**, *11*, 3863–3871.

[80] Zhang, C.; Pham, T. A.; Gygi, F.; Galli, G. Communication: Electronic structure of the solvated chloride anion from first principles molecular dynamics. *J. Chem. Phys.* **2013**, *138*, 181102.